J. Astrophys. Astr. (2018) 39:34
https://doi.org/10.1007/s12036-018-9524-7

OH megamasers: dense gas & the infrared radiation field

YONG HUANG[1,2,3], JIANGSHUI ZHANG[4,*], WEI LIU[4] & JIE XU[4]

[1] State Key Laboratory of Geodesy and Earths Dynamics, Institute of Geodesy and Geophysics, CAS, Wuhan 430077, China.
[2]University of Chinese Academy of Sciences, Beijing 100049, China.
[3]Physics Department, School of Science, Wuhan University of Technology, Wuhan 430070, China.
[4]Center for Astrophysics, Guangzhou University, Guangzhou 510006, China.
*Corresponding author. E-mail: jszhang@gzhu.edu.cn

MS received 11 February 2018; accepted 19 April 2018; published online 7 May 2018

Abstract. To investigate possible factors related to OH megamaser formation (OH MM, $L_{H_2O} > 10L_\odot$), we compiled a large HCN sample from all well-sampled HCN measurements so far in local galaxies and identified with the OH MM, OH kilomasers ($L_{H_2O} < 10L_\odot$, OH kMs), OH absorbers and OH non-detections (non-OH MM). Through comparative analysis on their infrared emission, CO and HCN luminosities (good tracers for the low-density gas and the dense gas, respectively), we found that OH MM galaxies tend to have stronger HCN emission and no obvious difference on CO luminosity exists between OH MM and non-OH MM. This implies that OH MM formation should be related to the dense molecular gas, instead of the low-density molecular gas. It can be also supported by other facts: (1) OH MMs are confirmed to have higher mean molecular gas density and higher dense gas fraction (L_{HCN}/L_{CO}) than non-OH MMs. (2) After taking the distance effect into account, the apparent maser luminosity is still correlated with the HCN luminosity, while no significant correlation can be found at all between the maser luminosity and the CO luminosity. (3) The OH kMs tend to have lower values than those of OH MMs, including the dense gas luminosity and the dense gas fraction. (4) From analysis of known data of another dense gas tracer HCO^+, similar results can also be obtained. However, from our analysis, the infrared radiation field can not be ruled out for the OH MM trigger, which was proposed by previous works on one small sample (Darling in ApJ 669:L9, 2007). On the contrary, the infrared radiation field should play one more important role. The dense gas (good tracers of the star formation) and its surrounding dust are heated by the ultra-violet (UV) radiation generated by the star formation and the heating of the high-density gas raises the emission of the molecules. The infrared radiation field produced by the re-radiation of the heated dust in turn serves for the pumping of the OH MM.

Keywords. Maser – galaxies—nuclei — galaxies—LIRGs — galaxies—dense gas — galaxies.

1. Introduction

OH molecular maser (emitting at $\lambda = 18$ cm) has been searched toward external galaxies for more than 40 years (Whiteoak & Gardner 1974; Baan *et al.* 1982) and the maser emission has been detected in 119 galaxies (Zhang *et al.* 2014). The maser emission among them is mostly extremely luminous with an isotropic luminosity larger than $10L_\odot$, which is million times more luminous than typical Galactic OH masers (hereafter taken as OH megamasers, OH MM). OH MM (normally the main line at 1667 MHz) have different properties from those of Galactic OH masers (Lockett & Elitzur 2008; Zhang *et al.* 2014), and should be a radically different phenomenon from the aggregate OH maser emission associated with normal (Galactic) modes of star formation in galaxies (Darling 2007).

OH MM host galaxies are luminous infrared galaxies (LIRGs, $L_{FIR} > 10^{11}L_\odot$), or even ultra luminous infrared galaxies (ULIRGs, $L_{FIR} > 10^{12}L_\odot$). And

This work was supported by the Natural Science Foundation of China (No. 11473007, 11590782).

statistical analysis also presents positive correlation between OH maser luminosity and the infrared luminosity of OH MM hosts (Martin *et al.* 1988; Baan *et al.* 1989; Kandalian 1996; Diamond *et al.* 1999; Darling & Giovanelli 2002). OH MMs are considered to be associated with major galaxy merger-induced starbursts, since the high infrared luminosity galaxies mostly show signs of interaction or merging from their optical imaging observations (Clements & Baker 1996). However, OH maser emission was not detected in the majority of (U)LIRGs ($\sim$ 80%). Thus other factors besides the infrared luminosity are necessary for the production of OH megamaser emission (Lo 2005).

Galaxy interaction or merging can provide conditions for OH MM formation, not only the strong infrared radiation field as pumping power, but also high density molecular gas in the merge nuclei. Molecular tracers of highly dense regions, including HCN, HNC, HCO^+, CS, CN, etc., have been observed toward (U)LIRGs, which were investigated and discussed completely by Baan *et al.* (2008). HCN molecule, one of the most abundant high dipole-moment molecules, is believed to be one of the best tracers of the dense gas, which requires about two orders of magnitude higher densities for collision excitation than CO ($n > 10^4 cm^{-3}$), (Gao & Solomon 2004a). And the number of HCN-detected galaxies is much more than that of other dense gas tracers. Gao & Solomon (2004a,b) carried out the first systematic HCN survey of a large local galaxy sample and got successful detections of HCN toward 52 galaxies. Before that, there were just 12 HCN-detected galaxies, since it was firstly detected in 1970s (Rickard *et al.* 1977). Based on those known 64 HCN-detected galaxies, Darling (2007) made a comparison analysis between OH MM sources and other star-forming galaxies and suggested that the dense gas is the OH MM trigger, instead of the infrared radiation field. However, the sample is small, with only 8 sources with OH MM detections.

Recently, all well-sampled HCN measurements in local galaxies were compiled and one big HCN sample was obtained (Liu *et al.* 2015). The big HCN sample and other additional sources with HCN detection and their physical parameters are collected here, to investigate possible factors for the OH MM formation, including the dense gas, the total molecular gas, the infrared radiation field etc. The sample and its corresponding data are briefly described in section 2. We presented our detailed analysis and results in section 3, including correlations between the infrared luminosity, the total molecular gas, the dense gas fraction, and OH maser emission etc. Section 4 summarizes our main results.

2. Sample and data

Our big HCN sample include 126 sources from Liu *et al.* (2015) and 6 additional HCN sources from reference (IRAS 12243-0036 and IRAS 15107+0724 from Baan *et al.* 2008; UGC 03374 from Curran *et al.* 2000; NGC 1377 from Imanishi *et al.* 2009; NGC 3607 and NGC 5866 from Crocker *et al.* 2012). We check firstly their information on OH megamaser survey (Darling & Giovanelli 2002; Zhang *et al.* 2014) and identify the OH MM, OH kMs, OH absorbers and OH non-detections. It includes 21 OH MMs, 11 OH kMs, 6 OH absorbing system and 95 non-OH MMs. All these sources with their physical parameters are collected and listed in Table 1, including the luminosity distance, the CO line luminosity (a proxy of the total molecular gas, L_{CO}), the infrared luminosity (a tracer of star formation rate, L_{IR}), the OH maser luminosity (L_{OH}) and the HCN line luminosity (a proxy of the dense gas, L_{HCN}). We have to mention, for several sources (see details in Table 1), the upper limit of L_{HCN} and L_{CO} can only be obtained from the original observation papers, instead of values given in Liu *et al.* (2015).

3. Analysis and discussion

3.1 *Star formation rate, gas emission of OH MMs and non-masers*

Taking the infrared luminosity L_{IR} as a tracer of star formation rate (SFR), we plot the L_{IR} against the molecular line luminosity L_{CO} and L_{HCN} for our HCN galaxy sample in Fig. 1a, b. The L_{CO} and L_{HCN} can be used as tracers of the low-density molecular gas and the dense molecular gas, respectively (Gao & Solomon 2004b). Similar to results in Gao & Solomon (2004b), one strong correlation appears in L_{IR}-L_{CO} (Fig. 1a) with a correlation coefficient of 0.72, and a stronger correlation in L_{IR}-L_{HCN} (Fig. 1b) with a correlation coefficient of 0.81. After removing the distance effect (using normalized luminosities), a significant correlation can be still found between L_{IR}/L_{CO} (a tracer of star formation efficiency) and L_{HCN}/L_{CO} (dense molecular gas fraction, Fig. 1d). While no obvious correlation exists between L_{IR}/L_{HCN} and L_{CO}/L_{HCN} (Fig. 1c). This means that the star formation rate indicated by L_{IR} depends on the dense molecular gas traced by HCN emission, not the low-density molecular gas traced by CO emission.

With respect to OH types, obvious difference can be found in Fig. 1. OH MMs tend to have both larger

Table 1. HCN galaxies with their parameters.

Source Name	RA (J2000)	DEC	D_L (Mpc)	$\log L_{IR}$ ($L_\odot$)	L_{CO} (10^8K km s^{-1} pc^2)	L_{HCN}	$\log L_{OH}$ ($L_\odot$)	Maser-Type
NGC 23	00 09 53.4	+25 55 26	62.4	11.08	16.23	0.65		Non
NGC 34	00 11 06.5	−12 06 26	80.92	11.46	35.32	8.97		Non
NGC 134	00 30 22.0	−33 14 39	21.38	10.62	3.76	<0.23		Non
IR00335-2732	00 36 00.5	27 15 34	281.69	11.94	<52.02	<29.89	2.61	Mega
NGC 174	00 36 58.9	−29 28 40	49.74	10.93	12.81	1.80		Non
NGC 253	00 47 33.1	−25 17 18	4.11	10.69	15.26	0.66	−1.5	Kilo
IR00506+7248	00 54 03.6	+73 05 12	65.2	11.44	22.81	0.78		Non
IC 1623	01 07 47.2	−17 30 25	80.72	11.65	118.73	7.36		Non
NGC 520	01 24 35.1	+03 47 33	30.59	10.92	28.84	0.62		Kilo
IR01364-1042	01 38 52.9	−10 27 11	205.92	11.83	48.23	12.11	2	Mega
NGC 660	01 43 02.4	+13 38 42	12	10.47	10.00	0.17		Non
III Zw 35	01 44 30.5	+17 06 05	110	11.57	18.55	2.70	2.65	Mega
NGC 695	01 51 14.2	+22 34 57	130.6	11.63	89.49	4.73		Non
NGC 828	02 10 09.6	+39 11 25	72.73	11.32	78.92	<0.77		Non
MRK 1027	02 14 05.6	+05 10 24	121.3	11.38	48.95	2.68		Non
NGC 891	02 22 33.4	+42 20 57	9.17	10.33	7.68	0.22		Non
UGC 1845	02 24 08.0	+47 58 11	63.96	11.08	19.79	1.09		Non
NGC 0931	02 28 14.5	+31 18 42	67.26	10.85	0.66	<1.00		Non
NGC 1022	02 38 32.7	−06 40 39	19.48	10.35	3.13	0.15		Non
NGC 1055	02 41 45.2	+00 26 35	13.63	10.25	10.09	<0.14		Non
Maffei 2	02 41 55.0	+59 36 15	4.1	9.73	6.72	0.09		Non
NGC 1068	02 42 40.7	−00 00 48	15.46	11.37	29.56	2.99	−1.6	Kilo
NGC 1144	02 55 12.2	−00 11 01	115.93	11.39	71.30	1.95		Non
IR03056+2034	03 08 30.7	+20 46 20	114.09	11.25	30.09	<0.60	1.28	Mega
NGC 1266	03 16 00.7	−02 25 38	29.7	10.48	13.64	0.52		Non
NGC 1365	03 33 36.4	−36 08 25	21.84	11.17	43.28	3.55	−0.15	Kilo
NGC 1377	03 36 39.1	−20 54 08	24.03	10.14		0.05		Non
IC 342	03 46 48.5	+68 05 47	4.32	10.11	16.32	0.40		Non
NGC 1530	04 23 27.1	+75 17 44	37.01	10.71	16.08	0.53		Non
NGC 1614	04 33 59.8	−08 34 44	64.78	11.61	32.86	1.25		Non
NGC 1667	04 48 37.1	−06 19 12	61.83	10.97	16.64	6.83		Non
NGC 1808	05 07 42.3	−37 30 47	12.56	10.71	6.63	0.70		Non
VII Zw 31	05 16 46.1	+79 40 13	220.72	11.92	226.41	10.69		Non
IR05189-2524	05 21 01.4	−25 21 45	173.26	12.10	67.85	6.59	2.16	Mega
IR05414+5840	05 45 47.9	+58 42 04	61.63	11.22	38.19	2.34	0.8	Kilo
UGC 03374	05 54 53.6	+46 26 22	85.45	11.10	5.93	<0.50		Non
NGC 2146	06 18 37.7	+78 21 25	15.34	11.00	14.34	1.03		Non
NGC 2273	06 50 08.6	+60 50 45	28.54	10.25	0.76	0.21		Non
NGC 2369	07 16 37.7	−62 20 37	44.72	11.10	27.09	1.97		Non
NGC 2276	07 27 14.3	+85 45 16	36.96	10.83	9.78	0.38		Non
NGC 2388	07 28 53.4	+33 49 09	60.4	11.25	22.85	1.14		Non
MCG+02-20-003	07 35 43.4	+11 42 34	69.15	11.08	9.90	0.51		Non
Mrk 10/UGC 04013	07 47 29.1	+60 56 01	122.84	10.78	4.38	<1.00		Non
IR08071+0509	08 09 47.2	+05 01 09	222.9	11.84	86.16	<4.62	2.25	Mega
He 2-10	08 36 15.1	−26 24 34	12	10.04		0.04		Non
NGC 2623	08 38 24.1	+25 45 17	76.71	11.52	24.47	1.41		Non
NGC 2764	09 08 17.4	+21 26 36	41.36	10.33	6.17	0.10		Non
Arp 55	09 15 55.1	+44 19 55	165.58	11.68	121.58	4.31		Non
NGC 2903	09 32 10.1	+21 30 03	8.53	10.22	5.16	0.15		Non

Table 1. continued

Source Name	RA (J2000)	DEC	D_L (Mpc)	$\log L_{IR}$ ($L_\odot$)	L_{CO} (10^8K km s^{-1} pc^2)	L_{HCN}	$\log L_{OH}$ ($L_\odot$)	Maser-Type
UGC 05101	09 35 51.6	+61 21 11	164.93	11.95	48.77	11.71	1.61	Mega
NGC 3032	09 52 08.1	+29 14 10	25.22	9.67	1.45	0.04		Non
NGC 3034 (M82)	09 55 52.7	+69 40 46	4.89	11.03	10.34	0.45		Kilo
NGC 3079	10 01 57.8	+55 40 47	19.51	10.79	29.68	1.22		Abs
NGC 3110	10 04 02.1	−06 28 29	73.24	11.29	24.74	1.02		Non
IR10039-3338	10 06 05.1	−33 53 17	143.7	11.71	32.83	7.69	2.92	Mega
NGC 3147	10 16 53.6	+73 24 03	43.05	10.93	61.65	0.64		Non
IRAS 10173+0828	10 20 00.2	+08 13 34	204		21.53	3.70	2.68	Mega
NGC 3256	10 27 51.3	−43 54 13	35.86	11.56	46.43	2.48		Non
IR10565+2448	10 59 18.1	+24 32 34	182.39	12.02	63.06	11.84		Non
NGC 3504	11 03 11.2	+27 58 21	26.36	10.69	10.89	0.64		Non
Arp 148	11 03 53.2	+40 50 57	147.13	11.60	45.54	4.84	2.02	Mega
NGC 3556	11 11 31.0	+55 40 27	12.09	10.24	3.69	0.10		Non
IC 0676	11 12 39.8	+09 03 21	21	9.69	1.09	0.02		Non
NGC 3620	11 16 04.7	−76 12 59	19.18	10.67	5.15	0.66		Non
NGC 3607	11 16 54.6	+18 03 06	10.27		0.30	0.02		Non
NGC 3627	11 20 14.9	+12 59 30	7.34	10.10	5.90	<0.03		Non
NGC 3628	11 20 17.0	+13 35 23	8.67	10.12	8.00	0.28		Abs
NGC 3665	11 24 43.7	+38 45 46	34.83	9.97	2.56	0.12		Non
Arp 299	11 28 30.4	+58 34 10	48.02	11.88	22.39	2.62	1.38	Mega
NGC 3893	11 48 38.2	+48 42 39	16.38	10.20	4.11	0.29		Non
IR11506-3851	11 53 11.7	−39 07 49	40.26	11.15	8.93	2.78	1.64	Mega
NGC 4030	12 00 23.6	−01 06 00	20.14	10.47	18.65	0.66		Non
NGC 4038	12 01 53.0	−18 52 03	21.1	10.82	12.52	0.16		Non
NGC 4041	12 02 12.2	+62 08 14	21.57	10.38	8.31	0.23		Non
IR12112+0305	12 13 46.0	+02 48 38	313.55	12.29	114.95	14.65	2.96	Mega
NGC 4414	12 26 27.1	+31 13 25	8.48	9.91	5.19	0.11		Non
IR12243-0036	12 26 54.6	−00 52 39	35.31	11.16	5.04	0.67	0.04	Kilo
NGC 4459	12 29 00.0	+13 58 42	19.53	9.48	0.52	0.06		Non
NGC 4526	12 34 03.1	+07 41 58	18.79	9.88	1.55	0.12		Non
NGC 4569	12 36 49.8	+13 09 47	18.8	10.20	16.25	0.23		Non
NGC 4631	12 42 08.0	+32 32 29	7.35	10.18	2.30	0.08		Non
NGC 4710	12 49 38.8	+15 09 56	19.23	9.88	2.20	0.11		Non
Mrk 231	12 56 14.2	+56 52 25	173.37	12.48	62.08	20.78	2.87	Mega
NGC 4826	12 56 43.6	+21 40 59	16.3	10.52	14.12	<0.26		Non
NGC 4945	13 05 27.5	−49 28 06	5.2	10.73	15.74	00.47		Abs
NGC 5005	13 10 56.2	+37 03 33	14.1	10.24	12.36	0.62		Non
NGC 5033	13 13 27.4	+36 35 38	12.63	10.06	6.19	0.17		Non
IR13126+2452	13 15 03.5	+24 37 08	54.08	11.09	16.90	<0.20	0.27	Kilo
NGC 5055	13 15 49.3	+42 01 45	7.44	10.03	6.35	<0.12		Non
Arp 193	13 20 35.3	+34 08 22	101.84	11.66	48.55	2.83		Abs
NGC 5135	13 25 44.0	−29 50 01	54.08	11.19	30.50	2.57		Non
NGC 5194	13 29 52.7	+47 11 43	7.53	10.29	14.00	0.06		Non
NGC 5236 (M83)	13 37 00.9	−29 51 56	4.7	10.33	7.07	0.06		Non
Mrk 266 SW	13 38 17.3	+48 16 32	121.77		76.16	0.61		Non
Mrk 266 (N5256)NE	13 38 17.5	+48 16 37	121.77	11.51		0.68		Non
Mrk 273	13 44 42.1	+55 53 13	159.66	12.14	66.72	14.35	2.55	Mega
NGC 5347	13 53 17.8	+33 29 27	32.18	9.95	0.39	<0.10		Non

Table 1. continued

Source Name	RA (J2000)	DEC	D_L (Mpc)	log L_{IR} ($L_\odot$)	L_{CO} (10^8K km s^{-1} pc^2)	L_{HCN}	log L_{OH} ($L_\odot$)	Maser-Type
NGC 5653	14 30 10.4	+31 12 56	55.31	11.05	16.44	0.63		Non
NGC 5678	14 32 05.6	+57 55 17	32.23	10.61	20.62	0.99		Non
NGC 5713	14 40 11.5	−00 17 20	30.26	10.82	11.33	0.38		Non
NGC 5775	14 53 57.6	+03 32 40	27.61	10.82	16.20	0.84		Non
NGC 5866	15 06 29.5	+55 45 48	12.93	9.54	0.43	0.03		Non
IR15065-1107	15 09 16.1	−11 19 18	28.5	10.49	4.13	0.12	0.31	Kilo
IR15107+0724	15 13 13.1	+07 13 32	61.57	11.30	10.95	2.04	1.06	Mega
NGC 5936	15 30 00.8	+12 59 22	55.4	10.97	12.38	0.60		Non
Arp 220	15 34 57.1	+23 30 11	80.89	12.20	90.59	10.78	2.59	Mega
NGC 6014	15 55 57.4	+05 55 55	34.34	9.71	1.87	0.05		Non
IR16399-0937	16 42 40.2	−09 43 14	113.18	11.52	37.00	<0.85	1.69	Mega
NGC 6240	16 52 58.9	+02 24 03	106.71	11.85	83.26	14.71		Abs
IRAS 17138-1017	17 16 35.8	−10 20 39	75	11.39	22.62	0.67		Non
IR 17208-0014	17 23 21.9	−00 17 01	175.81	12.35	115.15	16.38	3.04	Mega
IR17526+3253	17 54 29.4	+32 53 14	103.36	11.08	27.18	<0.94	0.99	Kilo
IRAS 18090+0130	18 11 33.4	+01 31 43	121.3	11.56	41.23	1.55		Non
IR18293-3413	18 32 41.1	−34 11 27	79.89	11.81	92.39	4.94		Non
NGC 6701	18 43 12.4	+60 39 12	59.07	11.07	32.51	1.30		Abs
NGC 6814	19 42 40.6	−10 19 25	21.5	10.15	1.80	0.18		Non
NGC 6921	20 28 28.8	+25 43 24	59.41	11.07	30.22	2.41		Non
NGC 6946	20 34 52.3	+60 09 14	4.16	9.94	5.16	0.23		Non
NGC 6951	20 37 14.1	+66 06 20	23.01	10.53	18.86	0.34		Non
IR20550+1656	20 57 23.9	+17 07 39	147.84	11.87	42.93	2.53	2.13	Mega
NGC 7130	21 48 19.5	−34 57 04	68.58	11.37	44.06	3.21		Non
IR22025+4205	22 04 36.1	+42 19 38	60.68	10.97	8.09	2.07	0.99	Kilo
IC 5179	22 16 09.1	−36 50 37	44.65	11.11	21.78	3.06		Non
NGC 7331	22 37 04.0	+34 24 56	14.38	10.56	27.11	0.37		Non
NGC 7465	23 02 01.0	+15 57 53	27.9	10.11	2.46	0.02		Non
NGC 7469	23 03 15.6	+08 52 26	68.08	11.61	33.31	2.01		Non
NGC 7479	23 04 56.6	+12 19 22	33.56	10.82	23.08	<0.59		Non
NGC 7552	23 16 10.7	−42 35 05	22.05	11.05	11.00	0.69		Non
NGC 7591	23 18 16.3	+06 35 09	67.37	11.01	16.45	0.57		Non
NGC 7582	23 18 23.5	−42 22 14	21.66	10.88	7.98	0.41		Non
IR23365+3604	23 39 01.3	+36 21 08	258.74	12.11	83.84	16.35	2.45	Mega
NGC 7771	23 51 24.8	+20 06 42	58.04	11.34	30.46	3.99		Non
Mrk 331	23 51 26.8	+20 35 10	71.92	11.41	42.55	2.76		Non

Note – All HCN galaxies include those from Liu *et al.* (2015) and other six sources (IRAS 12243-0036 and IRAS 15107+0724 from Baan *et al.* 2008; UGC 03374 from Curran *et al.* 2000; NGC 1377 from Imanishi *et al.* 2009; NGC 3607 and NGC 5866 from Crocker *et al.* 2012). Column 1: Source name; Cols. 2&3: Equatorial coordinates in J 2000; Col. 4: the distance in Mpc; Col. 5: the infrared luminosity ($8 - 1000\mu$m, logarithmic scale, in $L_\odot$). Cols. 6 & 7: L_{CO} and L_{HCN} are the CO and HCN line luminosities, mostly taken from Liu *et al.* (2015). The upper limits of luminosities were listed for several sources, which were derived from the observation data (Curran *et al.* 2000; Baan *et al.* 2008; Imanishi *et al.* 2009; Crocker *et al.* 2012). NGC 0931, its CO was detected with very low S/N (< 2) and its HCN was not detected (Curran *et al.* 2000). IR 00335-2732, both its CO and HCN were not detected (Baan *et al.* 2008), the upper limits are listed. These two sources were not included in our analysis. Col. 8: the isotropic OH maser luminosity in $L_\odot$, from Zhang *et al.* (2014); Col. 9: OH types as follows: "Mega" for Megamaser; "Kilo" for kilomaser; "Abs" for absorption; "non" for no OH lines detected

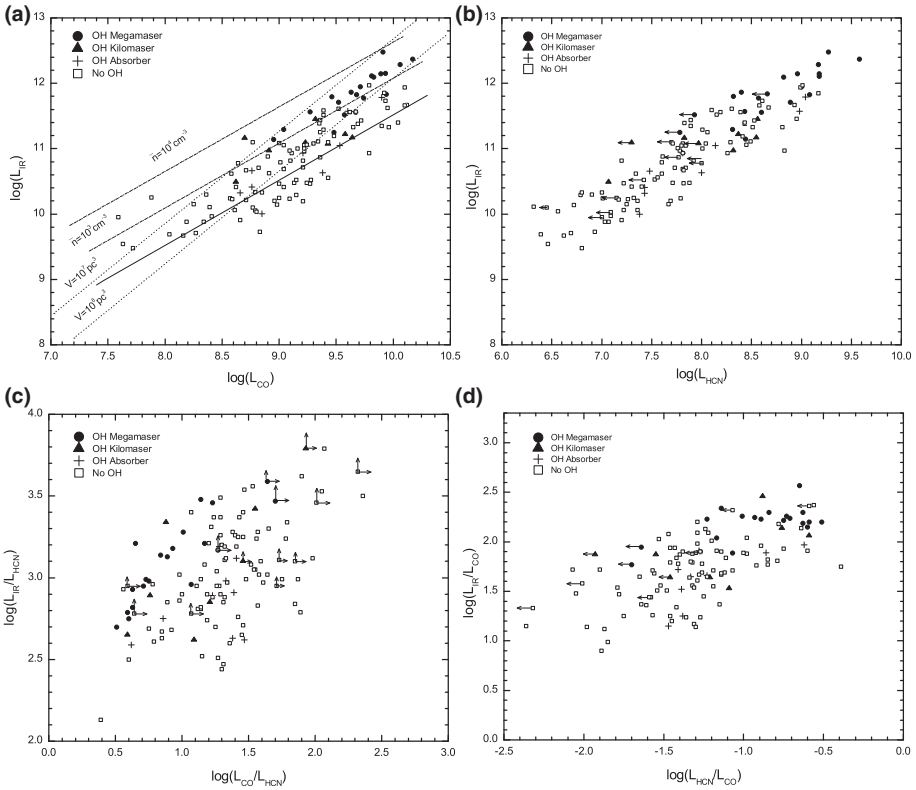

Figure 1. For the HCN-detected galaxy sample, their OH types (OH MMs, OH kMs, OH absorbers and sources with no OH detection) are indicted in different symbols (see the legend inside figure). (a) Infrared luminosity versus CO luminosity. Similar to Darling (2007), a solid line for linear fit (from Gao & Solomon 2004b, $\log \mathrm{L}_{IR} = \log \mathrm{L}_{CO} + 1.52$), dotted lines for constant total volume of molecular material and dashed lines for the mean H2 density are added. (b) Infrared luminosity versus HCN luminosity. (c) Normalized infrared luminosity v.s. CO luminosity (by L_{HCN}). (d) Normalized infrared luminosity v.s. HCN luminosity (by L_{CO}). Symbols with arrows indicate those sources with the upper limit of HCN luminosity (see details in section 2).

infrared luminosity (i.e., higher star formation rate) and larger HCN luminosity than other OH types, i.e., OH kMs, OH absorbers and non-OH MMs. While the difference on CO luminosity between them is not obvious. Like OH MMs, many non-OH MMs have also large CO luminosity (Fig. 1a). However in Figure 1b, few non-OH MMs have large HCN luminosity ($\log \mathrm{L}_{HCN} > 9$) as OH MMs, i.e., OH MMs tend to locate at regions with both larger L_{IR} and larger L_{HCN} than non-OH MMs. This demonstrates that the infrared radiation field and the dense gas, not the total molecular gas, should be related to OH MM emission.

Similar to Darling (2007), the L_{IR}-L_{CO} relation line (Gao & Solomon 2004b) and the mean H_2 density line (derived from Krumholz & Thompson 2007) are also plotted in Figure 1a. It shows that the non-OH MMs can basically follow the infrared-CO relation, while OH MMs locate mostly over the relation line. And OH MMs mostly have extremely high volume-averaged molecular densities ($10^3 \sim 10^4\,\mathrm{cm}^{-3}$). These results are similar to those of Darling (2007). Based on the fact that there are many non-OH MMs with high infrared luminosity at lower density and large volume than OH MMs, Darling (2007) concluded further that the dense gas is the trigger of OH MM and the infrared luminosity is not a condition for OH MM formation. However, as we can find, those non-OH MMs with lower density than OH MMs, at the same time, have lower L_{IR} (though relative high) than OH MMs (in both Darling 2007 and Figure 1 here). Thus this point is far from a firm conclusion, i.e., the infrared radiation field can not be ruled out for the OH MM trigger. Instead, the infrared radiation field should play one more important role on the OH MM trigger. On one hand, the UV generated by the star formation heats the molecules and its surrounding dust and the heating of the high-density gas raises the emission of the molecules. On the other hand, the infrared radiation field produced by the re-radiation of the dust heated by the UV associated with star formation provides the pumping energy of OH MMs and the pumping

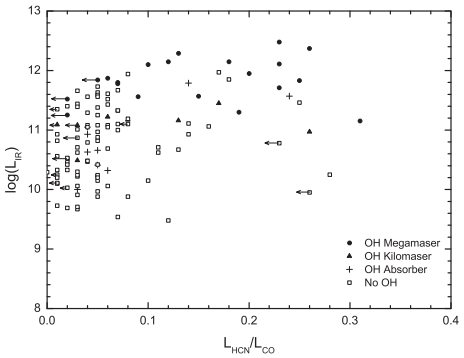

Figure 2. Infrared luminosity (L_{IR}) against the dense gas fraction (L_{HCN}/L_{CO}) for OH MMs and other HCN-detected sources. OH MMs tend to locate at regions with both large infrared luminosity and high dense gas fraction.

efficiency increases with the strength of the infrared radiation field. This is consistent with a stronger correlation in L_{IR}-L_{HCN}, than that in L_{IR}-L_{CO}. And it is clear that L_{IR} provides a threshold of $L_{FIR} > 10^{11} L_{\odot}$ for OH MM activity (Figure 1b).

Figure 2 presents the star formation rate ($\log L_{IR}$) against the dense gas fraction (L_{HCN}/L_{CO}) for the HCN-detected galaxy sample with known OH properties. OH MMs apparently prefer to LIRGs with large dense gas fraction, as found in Darling (2007). Darling (2007) found all 8 OH MMs have $L_{HCN}/L_{CO} > 0.07$ and just a few non-OH MM in this regime. For our big HCN sample, over 80% (17/ 21) OH MM objects have $L_{HCN}/L_{CO} > 0.07$, but only less than 25% (23/95) non-OH MMs with $L_{HCN}/L_{CO} > 0.07$. Especially, 7 of 11 sources with extremely large $L_{HCN}/L_{CO} (> 0.2)$ are OH MMs and one is OH kM. Here we have to mention that the large dense gas fraction should not reflect more dense gas HCN with respect to low-density CO, in the scenario of the dense gas heated by the UV from the starburst activity.

3.2 *OH MM and dense gas, infrared radiation field*

As suggested in section 3.1, besides the infrared luminosity, the dense molecular gas, not the low-density molecular gas, is related closely to OH MM formation. Here the relation between maser luminosity and gas luminosities are directly analyzed. The OH maser luminosity was plotted against CO luminosity (Fig. 3a) and HCN luminosity (Fig. 3b) for our HCN galaxy sample with maser detection, respectively. One significant correlation can be found for both panels, i.e., the rising maser luminosity with the increasing gas (for both low-density gas and dense gas) luminosity. And OH MMs have larger gas emission luminosity than OH kMs. However, the distance and galaxy size effect have to be considered for the luminosity-luminosity correlations (Gao et al. 2004a). Thus normalized luminosities were plotted again for both panels. For normalized L_{OH}-L_{CO} panel (Fig. 3c, L_{OH}/L_{HCN} v.s. L_{CO}/L_{HCN}), no obvious correlation can be found again and OH MMs do not have larger normalized CO luminosity than OH kMs at all. Nevertheless, for normalized L_{OH}-L_{HCN} panel (Fig. 3d, L_{OH}/L_{CO} v.s. L_{HCN}/L_{CO}), similar trend is still apparent, i.e., the rising normalized maser luminosity with the increasing dense gas luminosity, and OH MMs tend to have stronger dense gas emission than kMs. It supports that OH maser emission is related closely to the dense gas, instead of the low-density CO gas in maser host galaxy.

Further, besides HCN molecular, other dense gas tracers are necessary and deserved to be investigated and discussed. HCO^+, another typical tracer of the dense gas, was detected in 9 OH MM galaxies and 25 non-masing sources, according to the database in Baan *et al.* (2008). However, for other dense gas molecules (HNC, CN, CS etc.), there are just a few detections among our OH MM sample, which is difficult to do statistical analysis with reliable results. From analysis on HCO^+ detections, we got similar results: OH MMs tend to have strong dense gas emission than non-masing sources (also in figure 2 in Baan *et al.* 2008); the maser luminosity increases with rising HCO^+ emission luminosity. This confirms our previous conclusion from analyzing the dense gas HCN data, i.e., OH megamaser emission is related closely to the dense gas, instead of the low-density molecular gas.

Given that OH MMs are pumped by the far infrared radiation field (Skinner *et al.* 1997; Lockett & Elitzur 2008), the observed OH MM luminosity should be related to the infrared luminosity, $L_{OH} \propto L_{IR}^{\gamma}$. The power index $\gamma = 1$ and 2 represent a simple scenario of low-gain unsaturated and low-gain saturated masing, respectively (Darling & Giovanelli 2002). For our HCN-detected galaxy sample with OH megamaser emission, the OH MM luminosity was plotted against the infrared luminosity in Fig. 4. Similar to results in previous works (e.g., Baan *et al.* 1989; Diamond *et al.* 1999; Darling & Giovanelli 2002), one positive correlation is apparent and one linear fit gives $\log L_{IR} = (1.6 \pm 0.3) \log L_{OH} + (-17.4 \pm 2.9)$ for the entire sample, with a Spearman's rank correlation coefficient $R = 0.80$. This γ value ($1 < \gamma \leq 2$) supports an scenario that OH masers composed of many individual masing regions with different saturation states (Darling & Giovanelli 2002; Lo 2005).

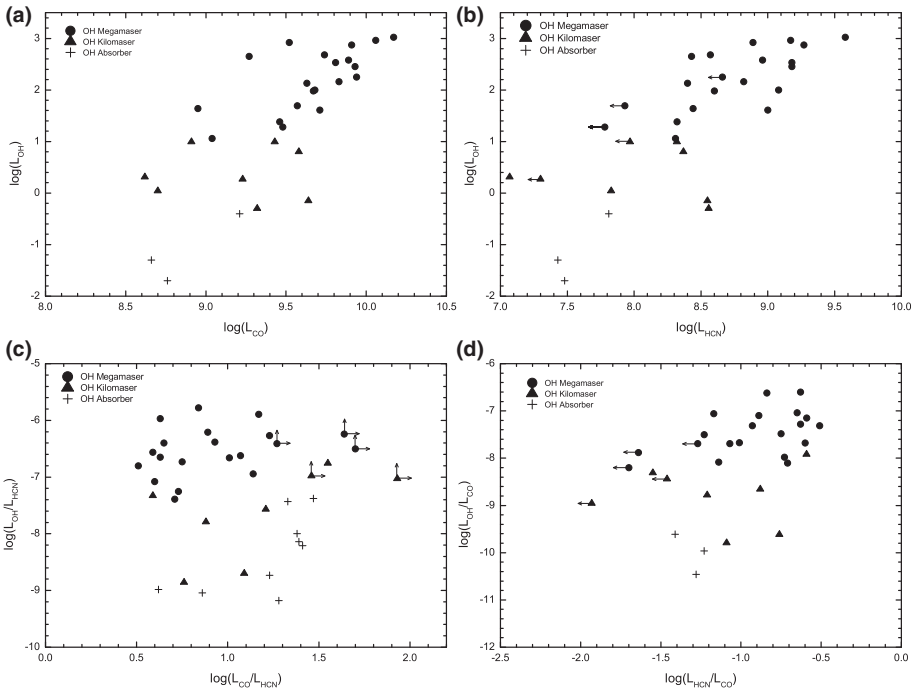

Figure 3. OH maser versus gas emission. (a) OH maser luminosity versus CO line luminosity. (b) OH maser versus HCN line luminosity. (c) Normalized OH maser luminosity v.s. CO luminosity (by L_{HCN}). (d) Normalized OH maser luminosity v.s. HCN luminosity (by L_{CO}).

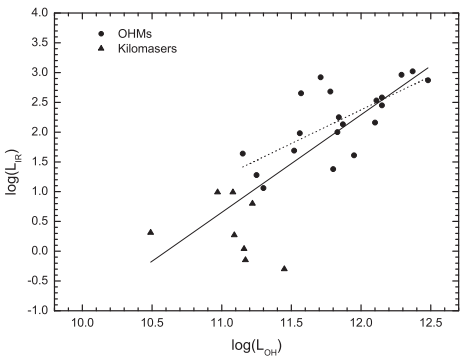

Figure 4. Infrared luminosity versus maser luminosity. The solid and dashed lines are linear fitting lines for all OH masers and megamaser alone, respectively. For OH MM alone, $\log L_{OH} = (1.1 \pm 0.3) \log L_{IR} + (-11.2 \pm 3.2)$, with a correlation coefficient ~ 0.7.

4. Summary

For all galaxies with dense gas HCN detections, their OH MM information was checked, to investigate possible factors for the OH MM formation, including the dense gas, the low-density molecular gas, the infrared radiation field etc. Our main results include:

(1) Relative to other HCN galaxies without OH megamaser, OH MM galaxies tend to have stronger HCN emission. This can be supported by analysis results on detections of another dense gas tracer HCO^+. However, no obvious difference on CO luminosity exists between OH MMs and non-OH MMs. Many non-OH MMs have large CO luminosity as OH MMs.

(2) For larger HCN sample with known OH properties than Darling (2007), OH MMs are confirmed to have higher mean molecular gas densities and higher dense gas fractions (L_{HCN}/L_{CO}) than non-OH MMs. However, the infrared radiation field can not be ruled out for the OH MM trigger. OH MMs locate at regions with both larger L_{IR} and larger L_{HCN} than non-OH MMs.

(3) After taking the distance effect into account, the apparent maser luminosity is correlated with the luminosity of the dense gas (both HCN and HCO^+), instead of that of the low-density molecular gas.

(4) The OH-FIR luminosity relationship is reexamined for our HCN sample with OH properties and one strong correlation is confirmed with $L_{IR} \propto {L^{1.6\pm0.3}}_{OH}$. This power index ($1 \sim 2$) suggests a mixture of saturated and unsaturated masers.

In summary, besides IR luminosity, the dense gas, instead of the low-density molecular gas, should be necessary for the production of the OH MM formation. This is consistent with the proposition that OH MMs are associated with galaxy merger or interaction. During the process of interaction, the UV generated by galaxy

merger-induced starburst heats the dense gas molecules and the heating of the high-density gas raises the emission of the molecules. And the infrared radiation field by the re-radiated of the dust, which was heated by the UV associated with starburst, provides pumping energy for the OH MM formation.

Acknowledgements

This work is supported by the Natural Science Foundation of China (No. 11473007, 11590782) and the State Foundation for Studying Abroad of China. We have made use of the NASA/IPAC Extragalactic Database (NED) which is operated by the Jet Propulsion Laboratory, California Institute of Technology, under contract with the National Aeronautics and Space Administration.

References

Baan, W. A., Wood, P. A. D., Haschick, A. D. 1982, ApJ, 260, L49
Baan, W. A., Haschick, A. D., Henkel, C. A. 1989, ApJ, 346, 680
Baan, W. A., Henkel, C., Loenen, A. F. et al. 2008, A&A, 477, 747
Clements, D. L., Baker, A. C. 1996, A&A, 314, L5
Crocker, A., Krips, M., Bureau, M. et al. 2012, ApJ, 421, 1298
Curran, S. J., Aalto, S., Booth, R. S. 2000, ApJS, 141, 193
Darling, J. 2007, ApJ, 669, L9
Darling, J., Giovanelli, R. 2002, AJ, 124, 100
Diamond, P. J., Lonsdale, C. J., Lonsdale, C. J. et al. 1999, AJ, 511, 178
Gao, Y., Solomon, P. M. 2004b, ApJS, 152, 63
Gao, Y., Solomon, P. M. 2004a, ApJ, 606, 271
Imanishi, M., Nakanishi, K., Tamura, Y., Peng, C. H. 2009, AJ, 137, 3581
Kandalian, R. A. 1996, Astrophys., 39, 183
Krumholz, M. R., Thompson, T. A. 2007, ApJ, 669, 289
Liu. L., Gao. Y., & Greve. T, R. 2015, Astrophys. J., 805, 31
Lo, K. Y. 2005, ARA&A, 43, 625
Lockett, P., Elitzur, M. 2008, ApJ, 677, 985
Martin, J. M., Bottinelli, L., Dennefeld, M. et al. 1988, A&A, 195, 71
Rickard, L. J., Turner, B. E., Palmer, P. et al. 1977, ApJ, 214, 390
Skinner, C. J., Smith, H. A., Sturm, E. et al. 1997, Nature, 386, 472
Whiteoak, J. B., Gardner, F. F. 1974, Astrophys. Lett, 15, 211
Zhang, J. S., Wang, J. Z., Di, G. X. 2014, A&A, 570, A110